

$\mathcal{O}(\alpha_s^2)$ corrections to $b \rightarrow c$ decay at zero recoil

J. Franzkowski⁽¹⁾ and J.B. Tausk⁽²⁾

(1) Institut für Physik, Johannes Gutenberg-Universität,
 Staudinger Weg 7, D-55099 Mainz, Germany

(2) Fakultät für Physik, Albert-Ludwigs-Universität Freiburg,
 Hermann-Herder-Straße 3, D-79104 Freiburg, Germany

Abstract

Analytic formulae are presented for the two-loop perturbative QCD corrections to $b \rightarrow c$ decay at the zero recoil point, which are required for the extraction of $|V_{bc}|$ from measurements of exclusive $B \rightarrow D^* l \nu$ decays. The results are in agreement with those in [8, 9]. Some comments on the numerical evaluation of the diagrams involved are made.

1 Introduction

The magnitude of the Kobayashi-Maskawa matrix element V_{cb} can be determined experimentally by observing the decays of B mesons produced in e^+e^- collisions. In particular, one method requires the measurement of the rate of the exclusive semileptonic decay $B \rightarrow D^* l \nu$ (see, e.g., [1]). From the decay rate, measured at the zero recoil point, i.e., in the special kinematical situation where the D^* is produced at rest in the B rest frame, one can then extract the value of $|V_{cb}|$. This method has been used by experiments where B mesons are produced on the $\Upsilon(4S)$ resonance [2] and on the Z resonance [3]. The statistical and systematic errors are currently of the order of 5%. However, in the future, with the CESR collider at Cornell running at increased luminosity, the asymmetric B factories at KEK and SLAC coming into operation, and further B -physics experiments to be conducted at the hadron accelerators Tevatron, HERA and LHC (see, e.g., [4]), the errors are expected to come down to around 1% or less [5]. Thus, it is important that the theoretical input, that is needed to extract $|V_{cb}|$ from the measured decay rates, be known with equal precision. The purpose of this paper is to present one component of that theoretical input, namely the second order perturbative QCD corrections to the decay of a b quark into a c quark at zero recoil. The other part of the theoretical input consists of non-perturbative corrections which are described by an expansion in the heavy quark masses m_b and m_c . For a review of heavy quark theory and further references, see, e.g., [6].

The reason for using the zero recoil point is that at that point, the non-perturbative contributions are suppressed by a factor of Λ_{QCD}^2/m_c^2 , because of an additional symmetry that exists in the infinite quark mass limit. At the same time, however, the zero recoil condition simplifies the kinematics of the decay $b \rightarrow cW$ to such an extent, that a complete analytical calculation of the perturbative corrections at the two-loop level becomes feasible.

At tree level, the amplitude for $b \rightarrow cW$ is proportional to $\bar{u}(c)\gamma^\mu(1 - \gamma_5)u(b)$. In higher orders, this gets modified into $\bar{u}(c)\gamma^\mu(\eta_V - \eta_A\gamma_5)u(b)$, where $\eta_{V,A}$ are given by perturbation series in α_s . (Only η_A enters the expression for $B \rightarrow D^*\ell\nu$.) At zero recoil, no other Lorentz structures appear. The order α_s contributions were calculated in [7]. The Feynman diagrams that contribute to $\eta_{V,A}$ in order α_s^2 are shown in figure 1. They were calculated analytically in [9], confirming the results of a Taylor series expansion in $(m_b - m_c)/m_b$ [8] that had been obtained earlier by one of the authors of [9]. In this paper, we present an independent analytic calculation of $\eta_{V,A}$. Although our results are expressed in a slightly different way, they are completely equivalent to the results of [9]. Thus, we confirm the conclusions of [8, 9].

Section 2 describes the main steps of the calculation. Although the details are different, the methods we have used are nevertheless related to the ones employed and extensively discussed in [9]. The major part of the work is the calculation of a set of scalar integrals, many of which contain infrared divergences. One example is looked at more closely, and various ways we checked our calculation are discussed. The final results are presented in section 3 and are followed by our conclusions in section 4. As a by-product of our work, we developed a new version of a numerical technique for evaluating a class of two-loop Feynman diagrams [10]. The new version is much more suitable for dealing with some of the rather special diagrams that occur in this calculation. However, because the method itself is quite general and may be useful for other problems as well, it is explained briefly in an appendix.

2 Calculation of $\eta_{V,A}$

An important consequence of the zero recoil condition is that there is no phase space available for gluon bremsstrahlung, $b \rightarrow cWg(g)$, and thus, only the virtual corrections shown in figure 1 are needed. We calculate them in the Feynman gauge and use dimensional regularization for both ultraviolet and infrared divergences. We neglect the masses of all the light quarks, and we leave out the diagram where a t quark loop is inserted into the gluon propagator. With these restrictions, all diagrams can be written in terms of the following nine propagator denominators:

$$\begin{aligned} P_1 &= (l+k).(2p_1+l+k), & P_3 &= l.(2p_1+l), & P_5 &= k.(2p_1+k), & P_7 &= k^2, & P_9 &= (l+k)^2, \\ P_2 &= (l+k).(2p_2+l+k), & P_4 &= l.(2p_2+l), & P_6 &= k.(2p_2+k), & P_8 &= l^2, \end{aligned} \quad (1)$$

where k and l are loop momenta and p_1 and p_2 are the four-momenta of the incoming b quark and the outgoing c quark, respectively. Normally, seven of the denominators P_i would be linearly independent, but because of the zero recoil condition, which means that p_1 and p_2 are proportional to each other, $m_2p_1 = m_1p_2$, we have two additional linear relationships between them:

$$m_1P_4 - m_2P_3 = (m_1 - m_2)P_8, \quad m_1P_6 - m_2P_5 = (m_1 - m_2)P_7. \quad (2)$$

This greatly simplifies the calculation.

After projecting the diagrams onto the form factors $\eta_{V,A}$ ¹ and expressing all scalar products of k , l , p_1 and p_2 that appear in the numerators in terms of the P_i , which we do using Form [11],

¹ In the case of η_A , we use an anticommuting γ_5 .

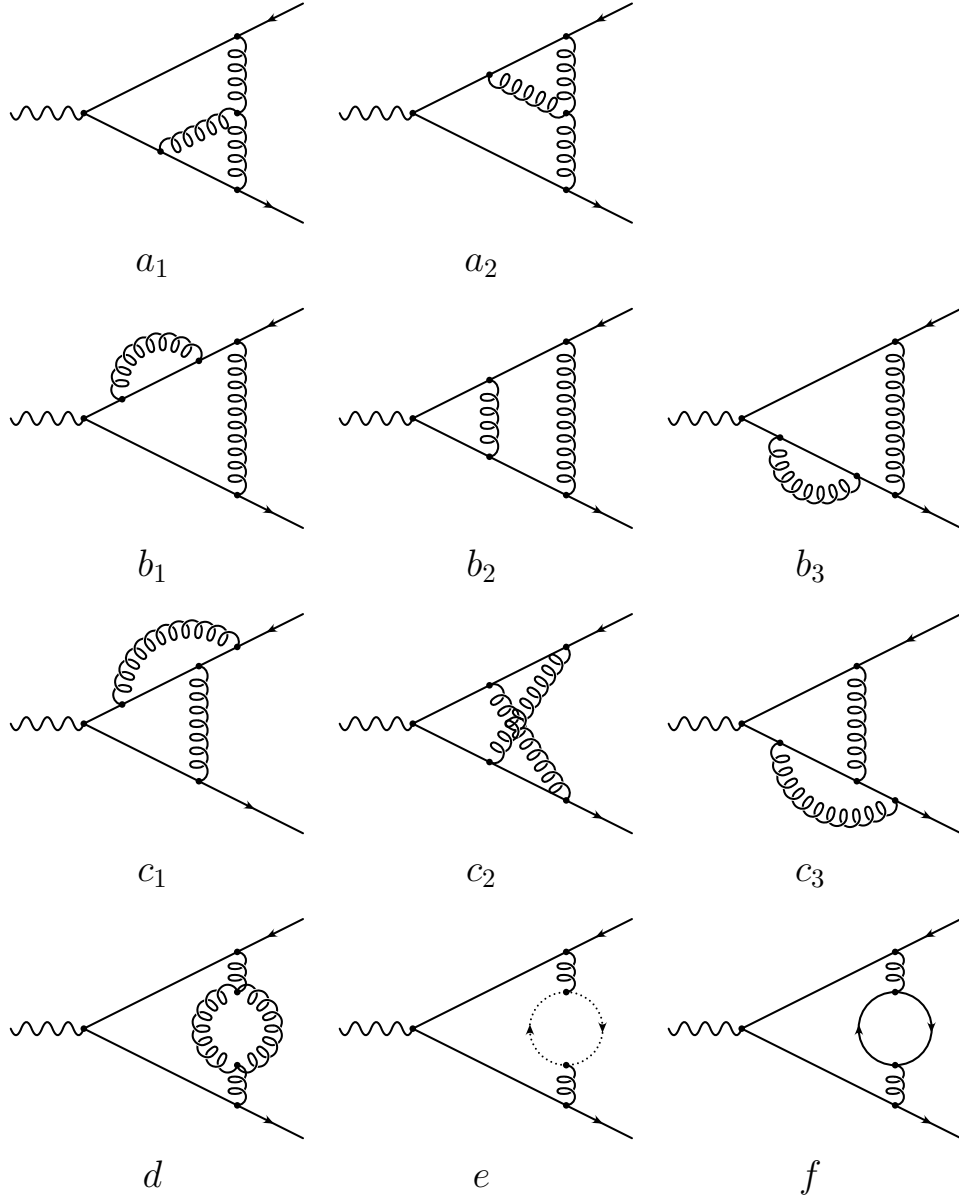


Figure 1: Irreducible Feynman diagrams contributing to $b \rightarrow cW$ at order α_s^2 . The dotted line in diagram e represents a Faddeev-Popov ghost. The fermion in the loop in diagram f can be either a light quark, a b or a c quark.

we obtain for each one a combination of scalar integrals of the form:

$$\int \int d^d k \, d^d l \, \frac{1}{P_1^{\nu_1} P_2^{\nu_2} \dots P_9^{\nu_9}}, \quad (3)$$

where $d = 4 - 2\epsilon$ (some of the ν_i can be negative). The scalar integrals that occur can be classified into three groups. The first group consists of integrals that can be factorized as a product of two one-loop integrals, e.g.:

$$\int \int d^d k \, d^d l \, \frac{1}{P_3 P_6 P_7 P_8} = \int d^d l \, \frac{1}{P_3 P_8} \times \int d^d k \, \frac{1}{P_6 P_7}. \quad (4)$$

The second group consists of integrals in which either $\nu_2 = \nu_4 = \nu_6 = 0$ or $\nu_1 = \nu_3 = \nu_5 = 0$, so that they only depend on one mass scale. Such integrals also occur in on-shell fermion self-energies and in anomalous magnetic moments, and can be calculated using recurrence relations based on integration by parts [12, 13]. A detailed explanation of the algorithm is given in [14].

The third group contains the non-factorizable graphs that depend on m_1 and on m_2 . Although one can still derive relations between them using integration by parts, those relations are more complicated than in the case of just one mass scale. We find them to be quite useful in a few cases, but are still left with rather a large number of cases we have to calculate from scratch.

Before actually calculating the remaining integrals in the third group, it is worth while to investigate their analytic properties by solving the Landau equations. One finds that they can have singularities when $m_1 = 0$ or $m_2 = 0$. At $m_1 = m_2$ there are no singularities because, although some poles in the propagators coincide at that point, the integration contours are not pinched. However, there may be singularities at $m_1 = m_2$ on the analytic continuation to higher Riemann surfaces. The following very simple one-loop example illustrates these properties:

$$\int d^d k \, \frac{1}{k \cdot (2p_1 + k) \, k \cdot (2p_2 + k)} = i\pi^{2-\epsilon} \Gamma(1 + \epsilon) \left(\frac{1}{\epsilon} + 2 - 2 \frac{m_1 \log(m_1) - m_2 \log(m_2)}{m_1 - m_2} \right) \quad (5)$$

If we analytically continue the right hand side of this equation in, say, m_2 , going around the branch point at $m_2 = 0$ and then back to $m_2 = m_1$, $\log(m_2)$ changes into $\log(m_2) + n(2\pi i)$, which no longer cancels $\log(m_1)$, and as a result, a pole appears at $m_1 - m_2 = 0$. In addition to the singularities just mentioned, a certain subclass of the two-loop integrals (3) can also have singularities when they are analytically continued to the point $m_1 + m_2 = 0$. The integrals in this subclass correspond to graphs that can be cut into two pieces by removing exactly three massive quark propagators. They only occur in diagrams c_1 , c_2 , and c_3 in figure 1, and in diagram f , when the quark in the loop is massive. While this discussion of analytic continuations to negative masses and higher Riemann surfaces may seem academic, keeping these properties in mind while actually doing the integrations can be very helpful, because it tells us which polylogarithms we can expect to occur in the answer.

We have done most of the integrals needed using Feynman parametric representations of the kind described in [15]. Sometimes, it is convenient to differentiate a diagram with respect to one (or both) of the masses first, in order to reduce the number of different kinds of propagators, and thus the number of Feynman parameters, and then reintegrate with respect to the mass to get the final answer. For the integration constant, we can take the equal mass point, which belongs to the second group discussed above. Another reason why we might want to differentiate with respect to masses, is to make an integral less infrared divergent.

Let us take the six-propagator integral

$$I_1(m_1, m_2) = \int \int d^d k \, d^d l \, \frac{1}{P_1 P_2 P_3 P_6 P_7 P_8} \quad (6)$$

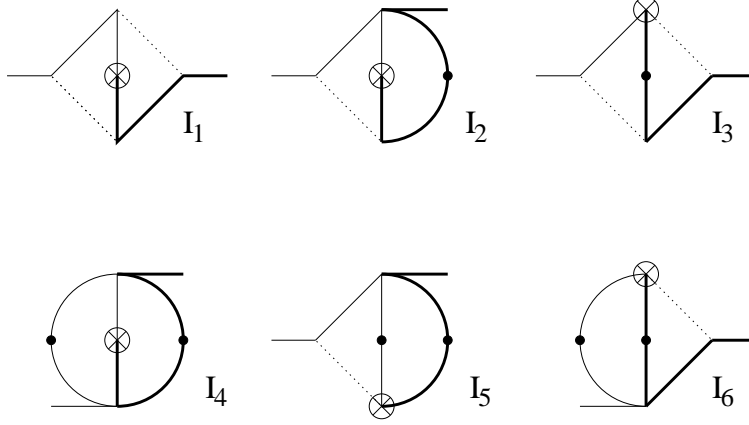


Figure 2: The scalar integrals $I_1 \dots I_6$. The momentum p_1 enters from the left, $p_2 - p_1$ enters at the vertex marked \otimes , p_2 leaves at the right. The thin (thick) lines symbolize quark propagators with mass m_1 (m_2). The dotted lines denote massless propagators. A line with a heavy dot on it means the corresponding propagator is squared.

shown in figure 2 as an example. It is one of the contributions that come from diagram c_2 in figure 1. This particular integral has no ultraviolet divergence, but it does contain an infrared divergence coming from the region where both k and l are small. Our goal is to express it in terms of other integrals in which one (or both) of the massless propagators P_7 and P_8 are cancelled. Let $p_{1,2} = m_{1,2}q$ where q is a fixed four-vector with $q^2 = 1$. First, consider differentiation with respect to m_2 . Using the identities,

$$\frac{\partial}{\partial m_2} \left(\frac{m_2}{P_6} \right) = \frac{P_7}{P_6^2} \quad (7)$$

$$\frac{\partial}{\partial m_2} \left(\frac{m_1 - m_2}{P_2} \right) = -\frac{P_1}{P_2^2}, \quad (8)$$

we get

$$\frac{\partial}{\partial m_2} \{ (m_1 - m_2) m_2 I_1(m_1, m_2) \} = (m_1 - m_2) I_2(m_1, m_2) - m_2 I_3(m_1, m_2), \quad (9)$$

where

$$I_2(m_1, m_2) = \int \int d^d k d^d l \frac{1}{P_1 P_2 P_3 P_6^2 P_8}, \quad (10)$$

$$I_3(m_1, m_2) = \int \int d^d k d^d l \frac{1}{P_2^2 P_3 P_6 P_7 P_8}. \quad (11)$$

The integral I_2 is already finite, but it can be simplified further by repeating the above procedure with m_1 instead of m_2 :

$$\frac{\partial}{\partial m_1} \{ (m_2 - m_1) m_1 I_2(m_1, m_2) \} = (m_2 - m_1) I_4(m_1, m_2) - m_1 I_5(m_1, m_2), \quad (12)$$

$$I_4(m_1, m_2) = \int \int d^d k d^d l \frac{1}{P_1 P_2 P_3^2 P_6^2}, \quad (13)$$

$$I_5(m_1, m_2) = \int \int d^d k d^d l \frac{1}{P_1^2 P_3 P_6^2 P_8}. \quad (14)$$

On the other hand, I_3 is still just as divergent as I_1 . However, since it no longer contains P_1 , it is now easy to cancel P_8 :

$$\frac{\partial}{\partial m_1} \{m_1 I_3(m_1, m_2)\} = I_6(m_1, m_2) = \int \int d^d k d^d l \frac{1}{P_2^2 P_3^2 P_6 P_7}. \quad (15)$$

From figure 2, it is obvious that $I_6(m_1, m_2) = I_5(m_2, m_1)$. Thus, in order to obtain the integral I_1 , all one needs to know are the two finite, four-propagator integrals I_4 and I_5 , which are relatively easy to do by Feynman parametrization, and, as an integration constant, the value of $I_3(m, m)$, which can be calculated by recurrence relations. Neglecting terms of order ϵ , we find

$$I_3(m, m) = \pi^d \Gamma^2(1 + \epsilon) \frac{m^{-4-4\epsilon}}{4} \left\{ \frac{1}{\epsilon} + 3\zeta(2) - 4 \right\}, \quad (16)$$

$$I_4(m_1, m_2) = \frac{\pi^4}{8m_1^2 m_2^2} \left\{ 3\zeta(2) - \frac{2}{u} (\text{Li}_2(u) - \text{Li}_2(-u)) + \frac{u^2 - 1}{u} \log\left(\frac{1+u}{1-u}\right) \right\}, \quad (17)$$

$$I_5(m_1, m_2) = \frac{\pi^4}{8m_1^2 m_2^2} \left\{ 2 - \frac{2}{u} - 3\zeta(2) + 2\text{Li}_2(u) - 2\text{Li}_2(-u) + \frac{1-u^2}{u^2} \log\left(\frac{1+u}{1-u}\right) \right\}, \quad (18)$$

where the dimensionless variable u is defined as $(m_1 - m_2)/(m_1 + m_2)$, and, after performing the final integrations over m_1 and m_2 ,

$$I_1(m_1, m_2) = \pi^d \Gamma^2(1 + \epsilon) \frac{m_1^{-2\epsilon} m_2^{-2\epsilon}}{4m_1^2 m_2^2} \left\{ \frac{1}{\epsilon} + 3\zeta(2) - 12 + \frac{2}{u} \left(\text{Li}_2(u) - \text{Li}_2(-u) + \log\left(\frac{1+u}{1-u}\right) \right) \right\}. \quad (19)$$

It is comforting to see that the result is symmetric in m_1 and m_2 , as it clearly should be.

We will not present formulae for all the non-factorizable two-mass scalar integrals (3) that appear in the diagrams of figure 1, but mention that they can all be expressed in terms of the following basic set of logarithms and polylogarithms:

$$\begin{aligned} & \log\left(\frac{1+u}{1-u}\right), \quad \log(1+u), \quad \text{Li}_2(u), \quad \text{Li}_2(-u), \quad \text{Li}_2\left(\frac{2u}{u+1}\right), \\ & \text{Li}_3\left(\frac{u}{u+1}\right), \quad \text{Li}_3\left(\frac{u}{u-1}\right), \quad \text{Li}_3\left(\frac{2u}{u+1}\right), \quad \text{Li}_3\left(\frac{2u}{u-1}\right), \quad \text{Li}_3\left(\frac{4u}{(u+1)^2}\right), \quad \text{Li}_3\left(\frac{-4u}{(u-1)^2}\right). \end{aligned} \quad (20)$$

These functions are all real and analytic in the range $-1 < u < 1$, which corresponds to real, positive masses m_1, m_2 . It is easy to verify that their only singularities are located at $u = \pm 1$, and in some cases $u = \infty$, in accordance with the general properties inferred above from the Landau equations. The functions that have branch points at $u = \infty$ only occur in diagrams with massive three-particle cuts, and the trilogarithms only occur in five-propagator integrals.

We applied various checks on the results for the scalar integrals. First of all, we evaluated the ones that are finite in $d = 4$ by direct numerical integration in momentum space, basically by a straightforward extension of the method originally proposed in [10] for the two-point two-loop “master” diagram with general masses. However, there are a few finite integrals that cannot easily be evaluated by this method, unless an important modification is made, which is explained in the appendix. Then, there are a number of “sunset” integrals, which we checked numerically by means of dispersion relations [16], and a few other two-point functions we compared with the program package Xloops [17].

A simple analytical check that can be applied to all two-mass integrals is to compare the first few terms of their Taylor expansions in u with what one gets by expanding the propagators around the equal mass point ($m_1 = m_2$) under the integral sign (as was done from the outset in [8]). While this is a powerful test, it is not sensitive to possible mistakes in the integration

constants in diagrams calculated by differentiating and then reintegrating with respect to the masses. Therefore, for some integrals, we also looked at their asymptotic behaviour in the limit when m_1 or m_2 vanishes ($u \rightarrow \mp 1$). In this limit, the diagrams are again reduced to one-scale integrals, but it is more complicated than the equal mass limit because, in general, the diagrams become more strongly divergent when one of the masses vanishes. Nevertheless, it is possible to obtain the correct asymptotic behaviour by expanding under the integral sign, provided one adds certain counterterms corresponding to the Taylor expansion of certain subdiagrams of the diagram considered, following the prescription for asymptotic expansions on the mass shell given in [18].

To conclude this list of consistency checks, we mention two tests that we applied to the contributions of complete diagrams, rather than individual scalar integrals. We verified that if m_1 and m_2 are interchanged, diagrams a_1 and a_2 in figure 1 are transformed into each other, and similarly $b_1 \leftrightarrow b_3$, $b_2 \leftrightarrow b_2$, $c_1 \leftrightarrow c_3$, $c_2 \leftrightarrow c_2$, $d \leftrightarrow d$, $e \leftrightarrow e$ and $f \leftrightarrow f$. This is a consequence of charge conjugation symmetry. Secondly, by putting the masses of the two external quarks equal to each other, we reproduced the two-loop on-shell quark wave-function renormalization constants in [13]. Except for one part — the contribution² of a quark loop whose mass is neither zero, nor equal to that of the external quark line — which we calculated separately, we could obtain all the wave-function renormalization factors by simply substituting $u = 0$ in our formulae for contributions to η_V .

3 Results

Here, we present our results for $\eta_{V,A}$ up to $\mathcal{O}(\alpha_s^2)$ in QCD with N colours and N_L flavours of massless quarks, but no t quarks. The colour factors are given by

$$C_A = N, \quad C_F = \frac{N^2 - 1}{2N}, \quad T_F = \frac{1}{2}. \quad (21)$$

Following [8, 9], we renormalize the strong coupling constant in the \overline{MS} scheme at the scale $M = \sqrt{m_b m_c}$ but use on-shell renormalization for the masses. This renormalization procedure has the nice property that it respects the symmetry under $m_b \leftrightarrow m_c$ mentioned at the end of the previous section. Therefore, $\eta_{V,A}$ are even functions of the variable:

$$u = \frac{m_b - m_c}{m_b + m_c}. \quad (22)$$

This symmetry was exploited in [8] by using the variable $\rho = (m_b - m_c)^2 / (m_b m_c) = 4u^2 / (1 - u^2)$ rather than $\delta = (m_b - m_c) / m_b = 2u / (1 + u)$ as an expansion parameter, in order to obtain a more rapidly converging series.

It turns out that the trilogarithms $\text{Li}_3\left(\frac{u}{u+1}\right)$ and $\text{Li}_3\left(\frac{u}{u-1}\right)$, which appear in the contributions of diagrams c_1 , c_2 and c_3 , cancel out in the sum $c_1 + c_2 + c_3$. The other functions (20) appear in the following combinations:

$$\ell = \log\left(\frac{1+u}{1-u}\right) \quad (23)$$

$$\mathcal{L}_1 = \text{Li}_2(u) - \text{Li}_2(-u) \quad (24)$$

$$\mathcal{L}_2 = \text{Li}_2\left(\frac{2u}{u+1}\right) + \frac{1}{4}\ell^2 \quad (25)$$

²Equation (22) in [13]

$$\mathcal{L}_3 = \text{Li}_3\left(\frac{2u}{u+1}\right) + \text{Li}_3\left(\frac{2u}{u-1}\right) + \frac{1}{6}\ell^3 + \frac{2}{3}\ell \text{Li}_2\left(\frac{2u}{u+1}\right) \quad (26)$$

$$\begin{aligned} \mathcal{L}_4 = & \text{Li}_3\left(\frac{4u}{(u+1)^2}\right) + \text{Li}_3\left(\frac{-4u}{(u-1)^2}\right) + \frac{4}{3}\ell^3 + \frac{16}{3}\ell \text{Li}_2\left(\frac{2u}{u+1}\right) \\ & - \zeta(2) (4\log(1+u) - 2\ell) - \frac{8}{3}\ell (\text{Li}_2(u) - \text{Li}_2(-u)). \end{aligned} \quad (27)$$

Note that ℓ , \mathcal{L}_1 and \mathcal{L}_2 are odd functions of u , while \mathcal{L}_3 and \mathcal{L}_4 are even. The abbreviations a and z_3 are defined by

$$a = \frac{\alpha_s(\sqrt{m_b m_c})}{4\pi} \quad (28)$$

$$z_3 = \zeta(3) - 4\log(2) \zeta(2). \quad (29)$$

Finally, the results are

$$\begin{aligned} \eta_V = & 1 + aC_F \left(\ell \frac{3}{u} - 6 \right) \\ & + a^2 \left[C_F T_F N_L \left\{ \ell \frac{(-\frac{2}{3})}{u} + \frac{4}{3} \right\} \right. \\ & + C_F T_F \left\{ \zeta(2) \frac{(-104u^2 + 464u^4 + 1144u^6 + 32u^8)}{(u^2 - 1)^4} + \ell \frac{(-\frac{64}{3} + \frac{200}{3}u^2 + \frac{344}{3}u^4)}{u(u^2 - 1)^2} \right. \\ & + \ell^2 \frac{(-16 + 224u^2 + 896u^4 + 416u^6 + 16u^8)}{(u^2 - 1)^4} \\ & + \mathcal{L}_1 \frac{(-32 + 128u^2 + 1616u^4 + 1312u^6 + 48u^8)}{u(u^2 - 1)^4} \\ & + \mathcal{L}_2 \frac{32 - 128u^2 - 2368u^4 - 3200u^6 - 480u^8}{u(u^2 - 1)^4} + \frac{\frac{128}{3} + \frac{296}{3}u^2 + \frac{344}{3}u^4}{(u^2 - 1)^2} \left. \right\} \\ & + C_F^2 \left\{ \zeta(2) \ell \frac{(-16)}{u} + \zeta(2) \frac{(-32 + 48u^2)}{u^2 - 1} + \ell \frac{(-\frac{89}{6})}{u} + \ell^2 \frac{3 - \frac{9}{2}u^2 + \frac{11}{2}u^4}{u^2(u^2 - 1)} \right. \\ & + \mathcal{L}_2 \frac{(-16)}{u(u^2 - 1)} + \mathcal{L}_3 \frac{24 - 96u^2}{u^2} + \frac{53}{3} \left. \right\} \\ & + C_F(C_A - 2C_F) \left\{ \zeta(2) \ell \frac{(-8u)}{u^2 - 1} + \zeta(2) \frac{10u^2}{u^2 - 1} + \ell \frac{\frac{17}{6}}{u} + \ell^2 \frac{2 + 2u^2}{u^2 - 1} \right. \\ & + \mathcal{L}_1 \frac{4u}{u^2 - 1} + \mathcal{L}_2 \frac{(-16u)}{u^2 - 1} - 24\mathcal{L}_3 + \mathcal{L}_4 \frac{12 - 6u^2}{u^2 - 1} + z_3 \frac{(-6u^2)}{u^2 - 1} - \frac{17}{3} \left. \right\} \Bigg] \end{aligned} \quad (30)$$

and

$$\begin{aligned} \eta_A = & 1 + aC_F \left(\ell \frac{3}{u} - 8 \right) \\ & + a^2 \left[C_F T_F N_L \left\{ \ell \frac{(-\frac{10}{3})}{u} + \frac{88}{9} \right\} \right. \\ & + C_F T_F \left\{ \zeta(2) \frac{(-64 - \frac{88}{3}u^2 + \frac{2512}{3}u^4 + \frac{2312}{3}u^6 + \frac{64}{3}u^8)}{(u^2 - 1)^4} \right. \\ & + \ell \frac{(-\frac{16}{3} + 120u^2 + \frac{136}{3}u^4)}{u(u^2 - 1)^2} + \ell^2 \frac{\frac{64}{3} + \frac{1120}{3}u^2 + \frac{2464}{3}u^4 + \frac{928}{3}u^6 + \frac{32}{3}u^8}{(u^2 - 1)^4} \end{aligned}$$

$$\begin{aligned}
& + \mathcal{L}_1 \frac{(-\frac{32}{3} + \frac{1472}{3}u^2 + \frac{4528}{3}u^4 + \frac{3104}{3}u^6 + 48u^8)}{u(u^2 - 1)^4} \\
& + \mathcal{L}_2 \frac{\frac{32}{3} - \frac{1664}{3}u^2 - \frac{8000}{3}u^4 - \frac{7808}{3}u^6 - \frac{992}{3}u^8}{u(u^2 - 1)^4} + \frac{\frac{1016}{9} + \frac{584}{9}u^2 + \frac{704}{9}u^4}{(u^2 - 1)^2} \Big\} \\
& + C_F^2 \left\{ \zeta(2) \ell \frac{(-16)}{u} + \zeta(2) \frac{(-48 + \frac{160}{3}u^2)}{u^2 - 1} + \ell \frac{(-\frac{53}{6})}{u} + \ell^2 \frac{(-\frac{4}{3} - \frac{5}{2}u^2 + \frac{31}{6}u^4)}{u^2(u^2 - 1)} \right. \\
& \left. + \mathcal{L}_2 \frac{\frac{16}{3} - \frac{32}{3}u^2}{u(u^2 - 1)} + \mathcal{L}_3 \frac{(-8 - 64u^2)}{u^2} - \frac{190}{9} \right\} \\
& + C_F(C_A - 2C_F) \left\{ \zeta(2) \ell \frac{\frac{32}{3} - \frac{56}{3}u^2}{u(u^2 - 1)} + \zeta(2) \frac{\frac{40}{3} - \frac{46}{3}u^2 + \frac{70}{3}u^4}{(u^2 - 1)^2} + \ell \frac{\frac{61}{6}}{u} \right. \\
& \left. + \ell^2 \frac{(-\frac{2}{3} + \frac{28}{3}u^2 + \frac{26}{3}u^4 + 4u^6)}{u^2(u^2 - 1)^2} + \mathcal{L}_1 \frac{\frac{32}{3} + \frac{52}{3}u^2 + \frac{44}{3}u^4}{u(u^2 - 1)^2} \right. \\
& \left. + \mathcal{L}_2 \frac{(-\frac{32}{3} - \frac{112}{3}u^2 - \frac{112}{3}u^4)}{u(u^2 - 1)^2} - 24\mathcal{L}_3 + \mathcal{L}_4 \frac{4 + 2u^2}{u^2 - 1} + z_3 \frac{4 - 10u^2}{u^2 - 1} - \frac{302}{9} \right\} \Big]. \quad (31)
\end{aligned}$$

Note that every single term in the expressions (30) and (31) is manifestly analytic in u for at least $|u| < 1$. This fact, combined with the symmetry $u \leftrightarrow -u$, proves (once more) that $\eta_{V,A}$ can be represented by convergent power series in u^2 for all finite positive values of m_b and m_c .

4 Conclusion

We have performed an independent calculation of the vector and axial vector form factors η_V and η_A that describe the decay of a b quark into a c quark at zero recoil up to order α_s^2 . We have compared our expressions (30) and (31) with the corresponding formulae in [9] by rewriting the latter in terms of the functions (20) used in this paper, and found that the two calculations are in perfect agreement. Both confirm the series expansion in the mass difference $m_b - m_c$ obtained earlier in [8].

The actual numerical values of m_b and m_c are such that a few terms of the series expansion are already sufficient to achieve the accuracy that is needed in practice ($u^2 \approx 0.29$). On the other hand, the exact analytical formulae are not only valid for $b \rightarrow c$ decays, but also for other cases, such as $t \rightarrow b$, where the mass ratio is larger, and the series expansion converges more slowly. They also allow one to study the limit when one of the quark masses goes to zero, which is impossible if only a limited number of terms of an expansion in the mass difference are known.

In the appendix, we have identified the cause of a numerical difficulty that arises when the two-dimensional numerical integration method of [10] is applied to certain two-loop diagrams with several coinciding thresholds, and suggested an alternative method that solves the problem.

We would like to thank J.G. Körner for suggesting this project and P. Post for helping us check some sunset diagrams. We are also grateful to A. Czarnecki, A.G. Grozin, K. Melnikov, M. Neubert and D. Pirjol for discussions. This work was partly supported by the Graduiertenkolleg “Elementarteilchenphysik bei mittleren und hohen Energien” at the Johannes Gutenberg University in Mainz.

Appendix

In this appendix, some details of the numerical integration methods we used to check the scalar two-loop integrals appearing in this work are given. We restrict ourselves to cases that are both

ultraviolet and infrared finite in $d = 4$. Basically, we follow the approach proposed in [10] for the numerical integration of the scalar two-point two-loop master diagram with general masses. The fact that the diagrams occurring here are three-point diagrams is not a problem: since the external momenta p_1 and p_2 are proportional to each other, they have a common rest frame, and all the steps in the derivation of the integral representation given in [10] can be repeated with only a few trivial changes in the formulae. However, the fact that p_1 and p_2 are on their respective mass shells does give rise to some difficulties, which we discuss here.

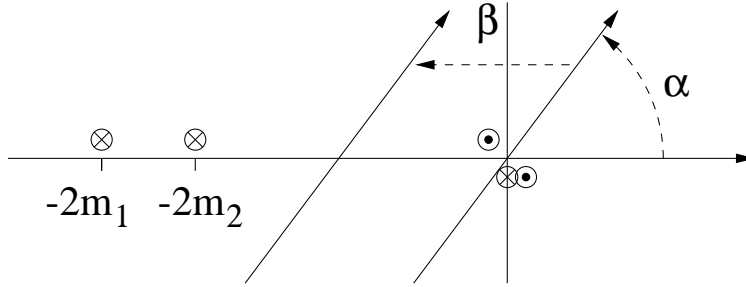


Figure 3: Singularities in the complex k_0 -plane originating from the quark propagators P_5 and P_6 (\otimes), and from the gluon propagator P_7 (\odot). While the integration contour can always be rotated away from the real axis by an angle α , it can only be shifted away from the origin in diagrams not containing the gluon propagator P_7 .

By writing the loop momenta k and l in the common rest frame of p_1 and p_2 as (k_0, \vec{k}_\perp) , (l_0, \vec{l}_\perp) , and integrating out their space components \vec{k}_\perp , \vec{l}_\perp , we obtain representations of the form

$$\int_{-\infty}^{\infty} \int_{-\infty}^{\infty} dk_0 dl_0 F(k_0, l_0; \rho) \quad (32)$$

for the scalar integrals (3). Here, we have explicitly indicated the dependence on the small imaginary quantity $i\rho$ which is added to all propagator denominators in accordance with the causal prescription. As a function of the complex variable k_0 , the integrand $F(k_0, l_0; \rho)$ has singularities (branch points) located at the positions shown in figure 3. Identical pictures can be drawn for the complex variable l_0 and for the combination $k_0 + l_0$. When the limit $\rho \rightarrow 0$ is taken, the singularities move onto the real k_0 and l_0 axes. In general, this makes the integrals along the real axes more difficult to evaluate numerically and in some cases even divergent. Sometimes, for example when the scalar integral under consideration does not contain either of the gluon propagators P_7 and P_9 , the problem can be solved by rotating the integration contours away from the real axes by an angle α (which must be the same for k_0 and l_0), $l_0 \rightarrow e^{i\alpha} l_0$, $k_0 \rightarrow e^{i\alpha} k_0$, and subsequently shifting (one of) them away from the origin, $e^{i\alpha} k_0 \rightarrow e^{i\alpha} k_0 - \beta$, as shown in figure 3. Scalar integrals we checked in this way include I_2 in figure 2 and $\int \int d^4k d^4l / (P_1 P_3 P_6^3 P_8)$.

This escape is not possible in diagrams where both the k_0 and l_0 contours are trapped at the origin by gluon propagators, such as, e.g.,

$$\int \int d^4k d^4l \frac{1}{P_1 P_3 P_6 P_7 P_8}. \quad (33)$$

We stress that if the limit $\rho \rightarrow 0$ is taken after all integrations have been performed, one obtains a finite result for the integral (33)³. However, one would like to set ρ to zero, or at least, very close to zero, *before* performing the k_0 and l_0 integrations in (32), and, if one attempts

³ In the case of equal masses $m_1 = m_2$, it reduces to the one difficult one-scale integral $N(1, 1, 1, 1) = 6 \zeta(2) \log(2) - \frac{3}{2} \zeta(3)$ needed in two-loop QCD or QED corrections to on-shell fermion propagators [19].

to do so, a non-integrable singularity appears at the point $k_0 = l_0 = 0$. More specifically, $F(\lambda k_0, \lambda l_0; \rho = 0) \sim 1/\lambda^2$ as $\lambda \rightarrow 0$. In the original integral (33), this logarithmic divergence comes from the region where \vec{k}_\perp and \vec{l}_\perp tend to zero, while k_0 and l_0 are of order $\vec{k}_\perp^2, \vec{l}_\perp^2$, as one can see by rescaling

$$\vec{k}_\perp \rightarrow \lambda \vec{k}_\perp, \quad \vec{l}_\perp \rightarrow \lambda \vec{l}_\perp, \quad k_0 \rightarrow \lambda^2 k_0, \quad l_0 \rightarrow \lambda^2 l_0. \quad (34)$$

Under this transformation, the integration measure in (33) scales like λ^{10} , while, for small λ , the integrand goes like $1/\lambda^{10}$.

The problem can be solved very easily by interchanging the order of the integrations. That is, we first perform the k_0, l_0 and all angular integrations analytically, leaving two integrations over $k_\perp = |\vec{k}_\perp|$ and $l_\perp = |\vec{l}_\perp|$ to be done numerically.

Below, we shall give an explicit formula for the resulting integrand. Although our main reason for deriving it was the need for an independent check on our analytic results for (33) and a few other, equally nasty cases, the formula is valid for a much more general diagram:

$$J = \int \int d^4k d^4l \frac{1}{D_1 D_2 D_3 D_4 D_5}, \quad (35)$$

where

$$\begin{aligned} D_1 &= (k + p_1)^2 - m_1^2 + i\rho & D_4 &= (l + p_4)^2 - m_4^2 + i\rho \\ D_2 &= (k + p_2)^2 - m_2^2 + i\rho & D_5 &= (l + p_5)^2 - m_5^2 + i\rho \\ D_3 &= (k + l + p_3)^2 - m_3^2 + i\rho. \end{aligned} \quad (36)$$

with the restriction that all momenta p_i are proportional to one another. Apart from that, the p_i and the masses m_i are arbitrary. Depending on the choice of the p_i , (35) then corresponds to a diagram with two, three or four external legs. We use this notation for the sake of flexibility, even though it has some redundancy (which could be used, for example, to set $p_2 = p_5 = 0$). Working in the rest frame of the momenta p_i , we find the following representation:

$$\begin{aligned} J = & 4\pi^4 \int_0^\infty dk_\perp \int_0^\infty dl_\perp k_\perp l_\perp \left\{ \frac{1}{u_1 u_4} \left(\frac{F_3^+(u_1 - p_1^0 + u_4 - p_4^0)}{C_{12}^+ C_{45}^+} + \frac{F_3^-(-u_1 - p_1^0 - u_4 - p_4^0)}{C_{12}^- C_{45}^-} \right) \right. \\ & \left. + (1 \leftrightarrow 2) + (4 \leftrightarrow 5) + (1 \leftrightarrow 2, 4 \leftrightarrow 5) \right\}, \end{aligned} \quad (37)$$

with

$$F_3^\pm(x) = \log \left(\frac{x + p_3^0 \pm u_3^+}{x + p_3^0 \pm u_3^-} \right), \quad (38)$$

$$C_{ij}^\pm = (\pm u_i - p_i^0 + p_j^0)^2 - u_j^2, \quad (39)$$

and

$$\begin{aligned} u_1 &= \sqrt{m_1^2 + k_\perp^2 - i\rho} & u_4 &= \sqrt{m_4^2 + l_\perp^2 - i\rho} \\ u_2 &= \sqrt{m_2^2 + k_\perp^2 - i\rho} & u_5 &= \sqrt{m_5^2 + l_\perp^2 - i\rho} \\ u_3^\pm &= \sqrt{m_3^2 + (k_\perp \pm l_\perp)^2 - i\rho}. \end{aligned} \quad (40)$$

The representation (37) can be applied directly as it stands to the case (33). In general though, there will be poles near the real axes at the points where the C_{ij}^\pm vanish. They can easily be avoided by a rotation of the contours: $l_\perp \rightarrow e^{-i\alpha} l_\perp$, $k_\perp \rightarrow e^{-i\alpha} k_\perp$.

References

- [1] J.D. Richman and P.R. Burchat, Rev. Mod. Phys. 67 (1995) 893.
- [2] ARGUS Coll. (H. Albrecht et al.), Z. Phys. C57 (1993) 533; CLEO Coll. (B. Barish et al.), Phys. Rev. D51 (1995) 1014.
- [3] OPAL Coll. (K. Ackerstaff et al.), Phys. Lett. B395 (1997) 128; DELPHI Coll. (P. Abreu et al.), Z. Phys. C71 (1996) 539; ALEPH Coll. (D. Buskulic et al.), Phys. Lett. B359 (1995) 236, B395 (1997) 373.
- [4] S. Stone, Syracuse preprint HEPSY 96-01 (hep-ph/9610305).
- [5] T. Kurimoto, Toyama preprint TOYAMA-96 (hep-ph/9706221).
- [6] I. Bigi, M. Shifman and N. Uraltsev, Notre Dame/Minneapolis preprint TPI-MINN-97-02-T (hep-ph/9703290).
- [7] J.E. Paschalis and G.J. Gounaris, Nucl. Phys. B222 (1983) 473.
- [8] A. Czarnecki, Phys. Rev. Lett. 76 (1996) 4124.
- [9] A. Czarnecki and K. Melnikov, Karlsruhe preprint TTP97-08 (hep-ph/9703277).
- [10] D. Kreimer, Phys. Lett. B273 (1991) 277.
- [11] J.A.M. Vermaseren, *Symbolic Manipulation with FORM* (Computer Algebra Nederland, Amsterdam, 1991).
- [12] N. Gray, D.J. Broadhurst, W. Grafe and K. Schilcher, Z. Phys. C48 (1990) 673; D.J. Broadhurst, Z. Phys. C54 (1992) 599; J. Fleischer and O.V. Tarasov, Comp. Phys. Comm. 71 (1992) 193; A. Czarnecki and A.N. Kamal, Acta Phys. Polon. B23 (1992) 1063.
- [13] D.J. Broadhurst, N. Gray and K. Schilcher, Z. Phys. C52 (1991) 111.
- [14] N. Gray, PhD. Thesis OUT-4102-35, Milton Keynes (1991).
- [15] R. Scharf, Diploma Thesis, Würzburg (1991); R. Scharf and J.B. Tausk, Nucl. Phys. B412 (1994) 523.
- [16] P. Post and J.B. Tausk, Mod. Phys. Lett. A11 (1996) 2115.
- [17] L. Brücher, J. Franzkowski, A. Frink and D. Kreimer, Nucl. Instrum. Meth. A389 (1997) 323; L. Brücher, J. Franzkowski and D. Kreimer, Mainz preprint MZ-TH/97-35 (hep-ph/9710484).
- [18] V.A. Smirnov, Phys. Lett. B394 (1997) 205.
- [19] D.J. Broadhurst, Z. Phys. C47 (1990) 115.